Electronic Supplementary Information

A Multicore Close-Packed Ultrathin-MnO_2@N-doped Carbon-Gear Yolk-Shell Micro-Nanostructures as Highly Efficient Sulfur Hosts for Li-S Batteries

*Weixi Yan[†a], Shipei Chen[†a], Ming Wen[*a], Qingsheng Wu[a], Shuhong Yu[*b]*

[a]School of Chemical Science and Engineering, Shanghai Key Laboratory of Chemical Assessment and Sustainability, Tongji University, Shanghai 200092, P. R. China.
E-mail: m_wen@tongji.edu.cn

[b]Department of Chemistry, University of Science and Technology of China, Hefei National Laboratory for Physical Sciences at the Microscale, Jinzhai Road 96, Hefei 230022, P. R. China.
E-mail: shyu@ustc.edu.cn

[†] These authors contributed equally to this work.

Keywords:

Clustered MnO_2-S@NC-gear composite, Yolk-shell nanostructure, Cathode material, Li-S battery

Experimental section

Chemicals:

All chemicals used in this work were of analytical grade and were directly used without further purification.

Preparation of the Ultrathin-MnO_2:

Typically, purification, the ultrathin-MnO_2 was synthesized by a "Baeyer test for unsaturation" reaction.[1] $KMnO_4$ (1 g) was dissolved in deionized water (500 mL). Then oleic acid (10 mL) was added with mechanical stirring for 2 hours. The black products were collected by washed by water and ethanol, respectively.

Preparation of the clustered MnO_2@CG and MnO_2@NCS Composite:

As contrast samples, the monodispersed MnO_2@NCG composites were synthesized under the same process as illustrated in preparation of the multicores close-packed MnO_2 @NCG composite (Experiment section) in body content without the first addition of TEOS; the preparation of MnO_2@CG has similar synthesis condition except for the addition of ethane diamine (2 mL); the multicores close-packed MnO_2@NCS could be gained under the above process without the second addition of TEOS.

Preparation of the NCG and CG

Preliminary products SiO_2 were obtained via a Stöber synthesis method. TEOS (0.5ml), resorcinol (40 mg), formaldehyde (37 wt%, 0.056 mL) and ethane diamine (2 mL) were added into the mixed solution composed of ammonia (28wt%,1 mL) and SiO_2 (100 mg), deionized water (30 mL). After vigorously stirring for 2 hours, the product N-doped carbon-internal-gear (NCG) was then centrifugally washed and dried at 60℃. If the TEOS was not been added, the N-doped carbon smooth shelled hollow spheres (NCS). And the CG would be acquired when removed the ethane diamine during the process described above.

Supporting Tables and Figures

Table S1. BET specific surface, pore volume and BHJ average pore dimeter of MnO_2.

Samples	Specific surface area	Pore Volume	Pore Dimeter
	$m^2\ g^{-1}$	$cm^3\ g^{-1}$	nm
MnO_2	208.93	0.92	10.35

Table S2. The simulation results of the equivalent circuit and EIS spectra in Figure 3D.

Samples\Impedance	Rct / Ω	Std. error
MnO_2-S@GNC	18.9	1.3
MnO_2-S@GC	74.02	3.2
MnO_2-S	111.5	2.9
S	208.9	2.3

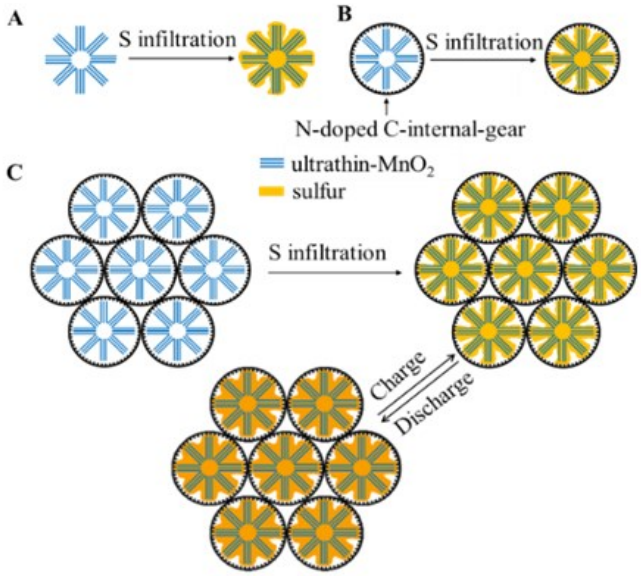

Scheme S1. Design strategy of the clustered MnO_2-S@NCG.

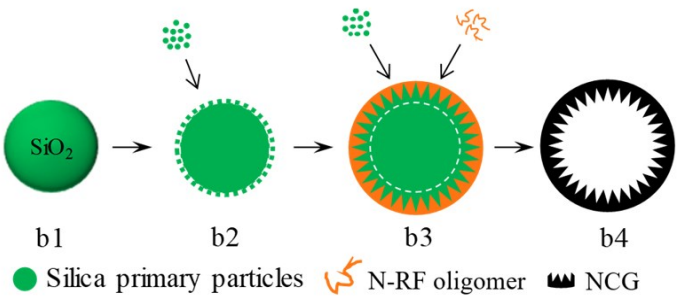

Fig. S1. Schematic illustration of the synthesis process of NCG.

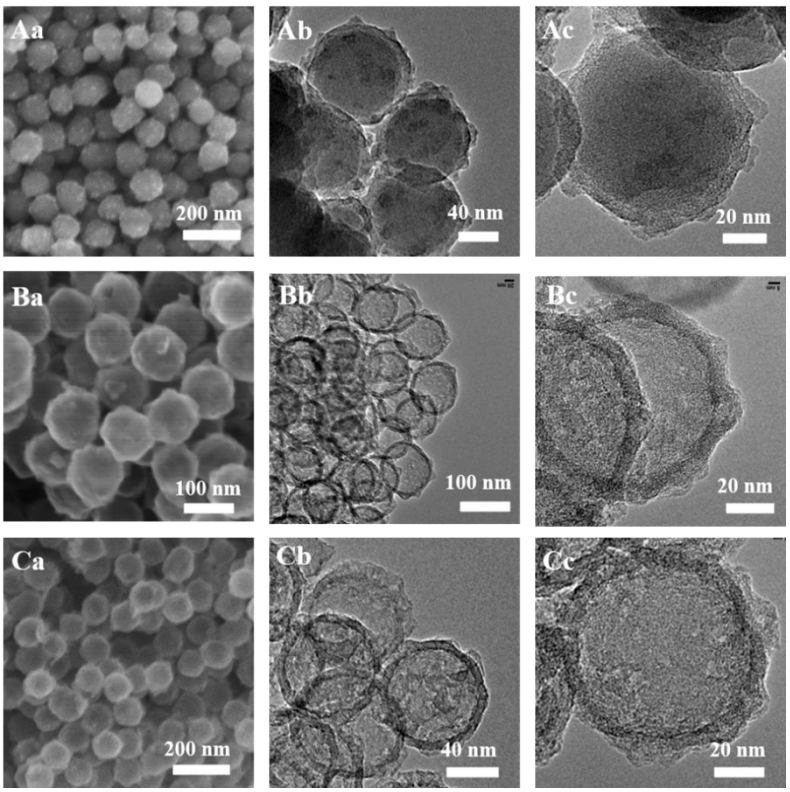

Fig. S2 (A) SEM image (a), low (b) and high (c) magnifiction TEM images of SiO_2@SiO_2-N-RF; (B) SEM image (a), low (b) and high (c) magnifiction TEM images of NCG after carbonization and etching SiO_2; (C) SEM image (a), low (b) and high (c) magnifiction TEM images of CG.

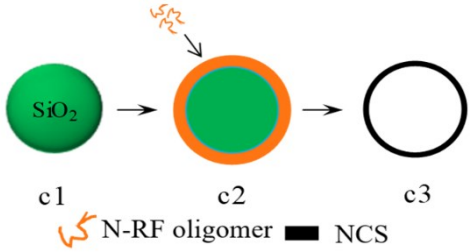

Fig. S3. Schematic illustration of the synthesis process for NCS.

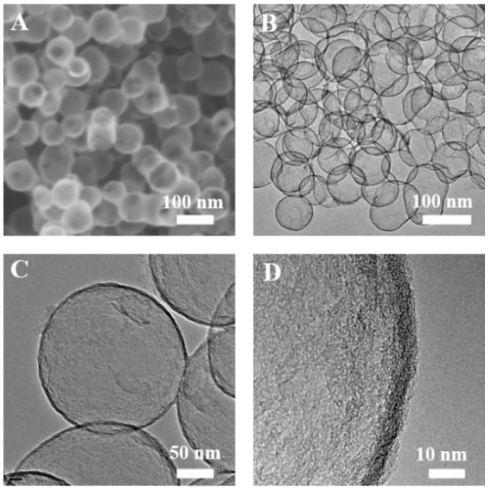

Fig. S4. (A) SEM image and (B-D) TEM images of NCS at different magnification.

Note: Based on the synthesis mechanism of the gear liked carbon hollow spheres, using SiO_2 nanospheres as hard templates through the similar process of the synthesis of MnO_2@NCG (Exp. section), the hollow N-doped internal C-gear (NCG) spheres could be obtained. In Fig. S2A, the SEM and TEM images show that the average diametre of the SiO_2@SiO_2-N-RF spheres is about 100 nm. After etching SiO_2, the morphology and structure of NCG keep stably, besides, there are gear liked carbon spikes on the inner surfae of the NCG (Fig. S2B). In addition, the size of hollow is determined mainly by the size of the original hard template. So the NCG shell can be successfully obtained in this work. As a contrast the N-doped carbon smooth-shelled-hollow-spheres (NCS) has been synthesised via SiO_2 as hard template then added N-RF alone, the Schematic illustration of the synthesis process and the morphology were shown in Fig. S3 and Fig. S4.

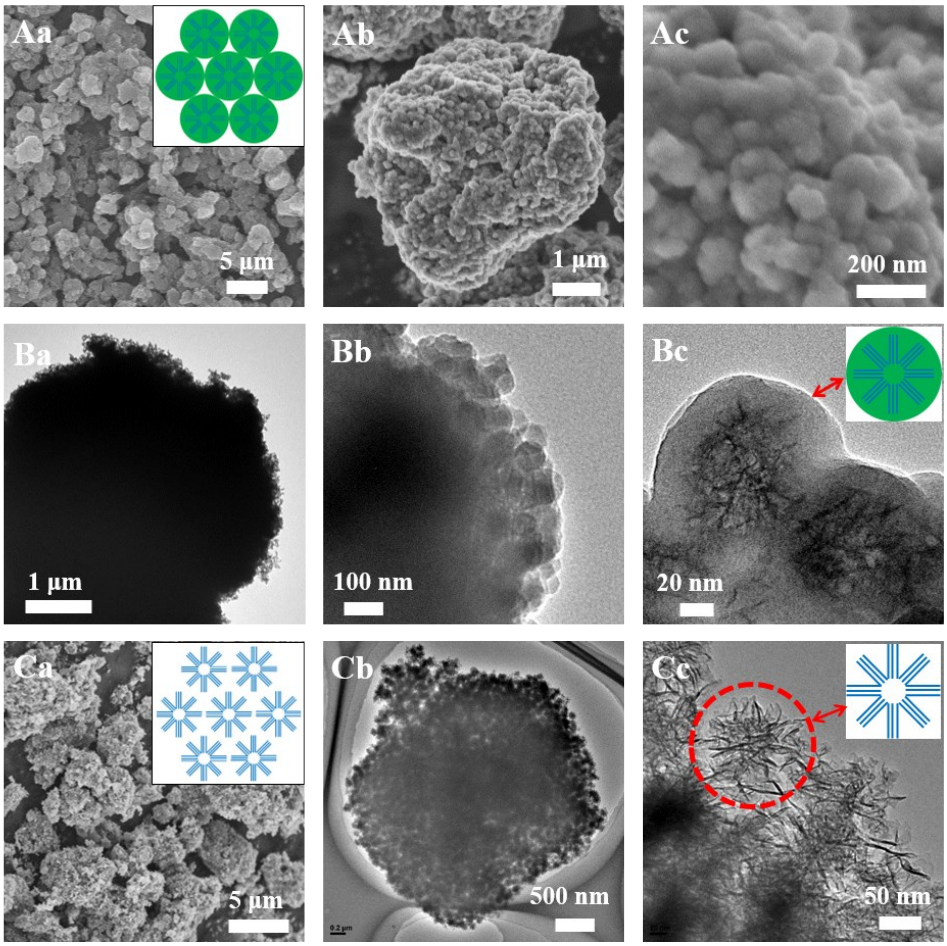

Fig. S5. (A) SEM and (B) TEM images of the clustered MnO_2@SiO_2 at different magnification; (C) The clustered ultrathin-MnO_2: (A) SEM, (B) TEM images at different magnification.

Note: There have been studies on the preparation of microemulsion spheres by using emulsion stabilizer to aggregate monodisperse nano-spheres, and the size of the final aggregation product can be controlled by controlling the diameter of emulsion spheres.[2] The disadvantage of this method is that the preparation process is complicated, which requires extremely high stirring speed and temperature treatment. Herein, a one-step method was developed to successfully prepare multicores close-packed composite.The experimental process may be as follows: with the help of surfactant CTAB, the nanometer ultrathin-MnO_2 self-assembly into micronspheres, while TEOS hydrolyzed on the MnO_2 to generate SiO_2 then wrap it. In Figure S5A-B, the MnO_2@SiO_2 composite with good dispersion and a particle size of 3~5 μm consists of nanospheres (~100 nm). From TEM images (Fig. S5Ba), it can be further observed that clustered MnO_2@SiO_2 microspheres are closely packed and grown by small MnO_2@SiO_2

nanospheres, and the formation mode is shown in the two-dimensional illustration in the inste of Fig. S5Aa. The higher magnification TEM image (Fig. S5Bb) further shows that the ultrathin-MnO_2 is wrapped by SiO_2 externally, with a thickness of about 20 nm. In order to further study the internal structure composition, SiO_2 was etched and the morphology of products was shown in Fig. C. Firstly, after etching, the morphology of the micron sphere is maintained and uniformly dispersed, as shown in the two-dimensional illustration in the inset of Fig.S5 Ca. Furthermore, as can be seen from the TEM images, there are spaces inside the micron sphere, indicating that the material is uniform aggregation of ultrathin-MnO_2. Besides, a single ultrathin-MnO_2 can also be clearly seen in the high magnification TEM image (Fig. S5 Cc).

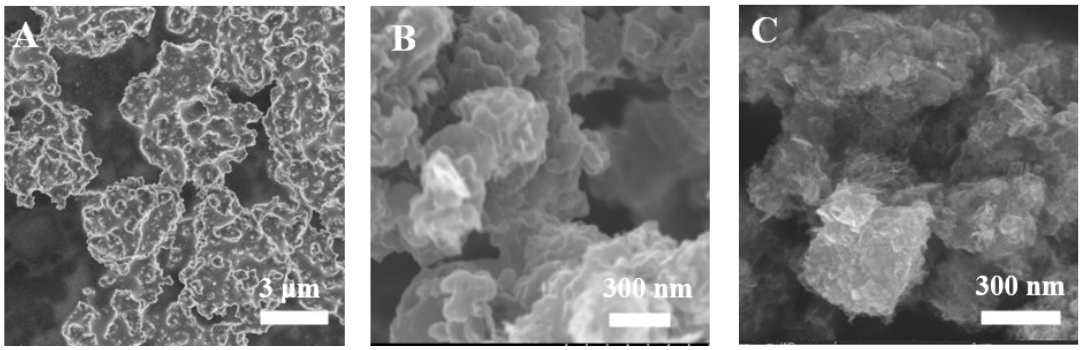

Fig. S6. SEM images the clustered MnO_2@SiO_2@SiO_2/N-RF(A); MnO_2@NCG (B) after carbonization and ecting SiO_2 ; the clustered MnO_2-S@NCG (C) without residual sulfur on the surface.

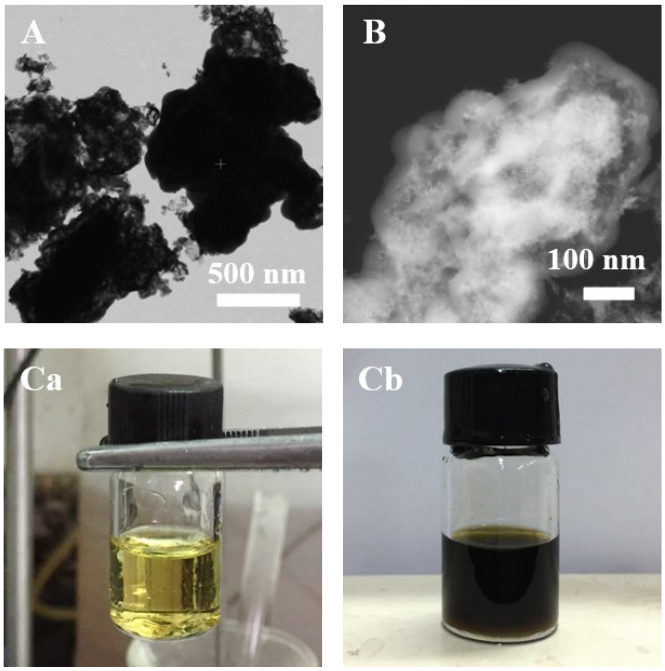

Fig.S7. (A, B) STEM images of MnO_2-S@NCG in bright and dark field; (C) Photographs of the valid S solution infiltration process of sulsur-CS_2 solution (a) and MnO_2-S@NCG-CS_2 solution (b).

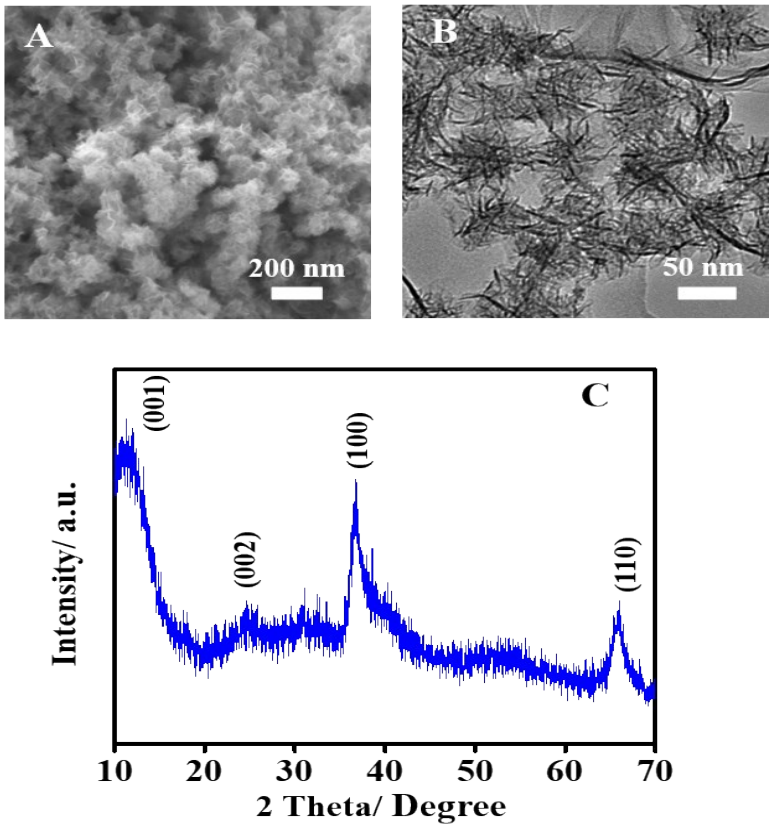

Fig. S8. The ultrathin-MnO_2 : (A) SEM, (B) TEM images; (C) XRD pattern.

Note: The X-ray diffraction (XRD) pattern was invetigated in the range of the diffraction angle (2θ) of 10~70° shown in Fig. S8C. The diffraction peaks at 2θ=12.3, 24.3, 36.6, 65.7° correspond to the crystal plane (001), (002), (100), and (110) of the monoclinic birnessite MnO_2 crystal structure (JCPDS 80-1098),[3] respectively, indicating that the ultrothin-MnO_2 owns layered structure. Moreover, from 2θ=12.3°, the crystal plane spacing is calculated to be 0.72nm, consistent with HRTEM results.

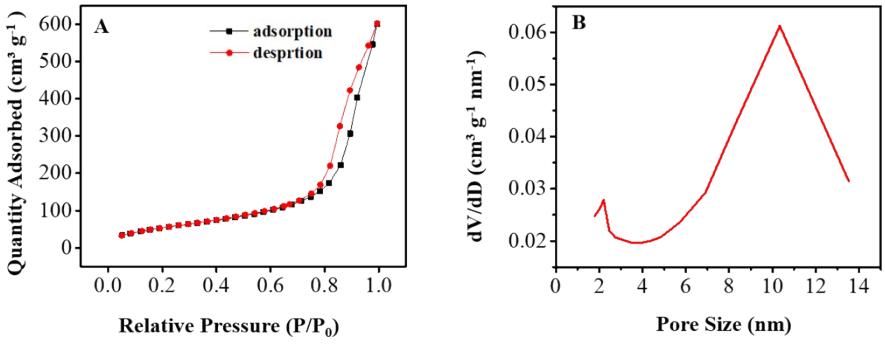

Fig. S9. (A) N_2 adsorption-desorption isotherms for MnO_2; (B) The corresponding pore size distributions.

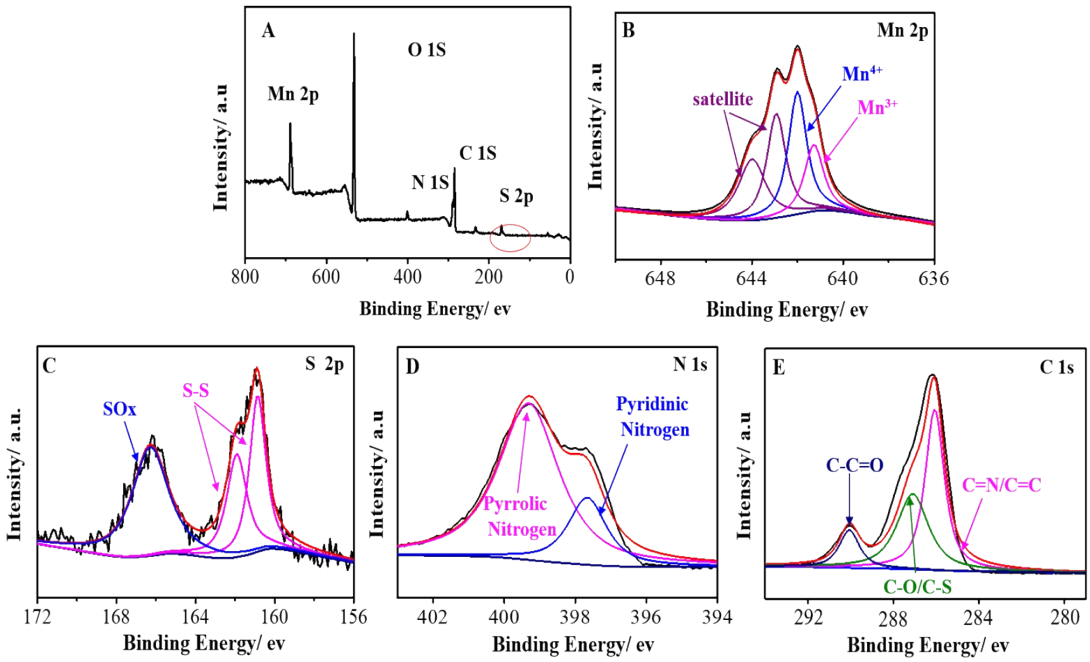

Fig. S10. XPS spectra of MnO_2-S@NCG: (A) full survey spectrum, (B-E) high-resolution spectra for Mn 2p, S 2p, N 1s, C 1s, respectively.

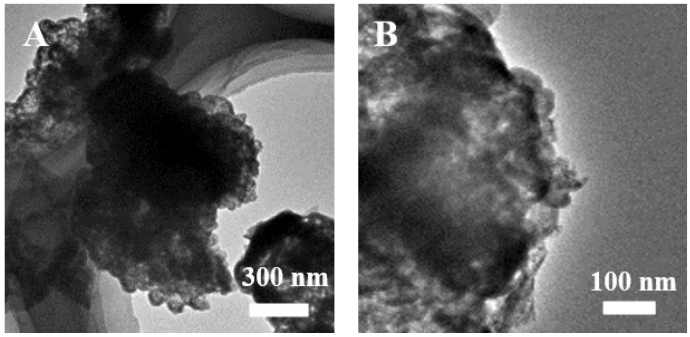

Fig. S11. SEM and TEM images of MnO_2-S@NCS at different magnification.

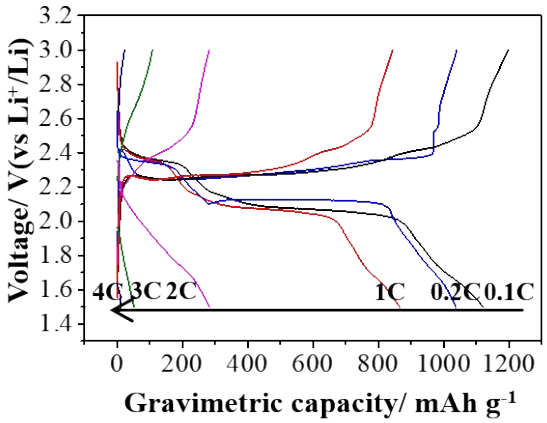

Fig. S12. Discharge-charge voltage profiles of MnO_2-S@NCS at various rates.

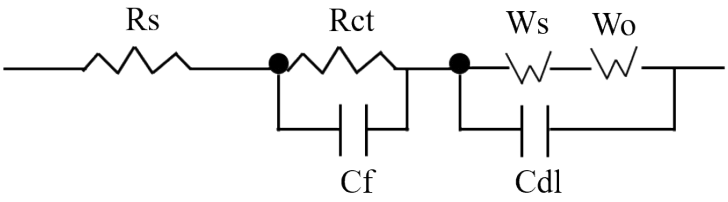

Rs: series resistance; Rct: charge-transfer resistance;
Ws: adsorption impedance; Wo: the semi-infinite Warburg diffusion impedance.

Fig. S13. The corresponding equivalent circuit of Nyquist plots for MnO_2-S@NCG.

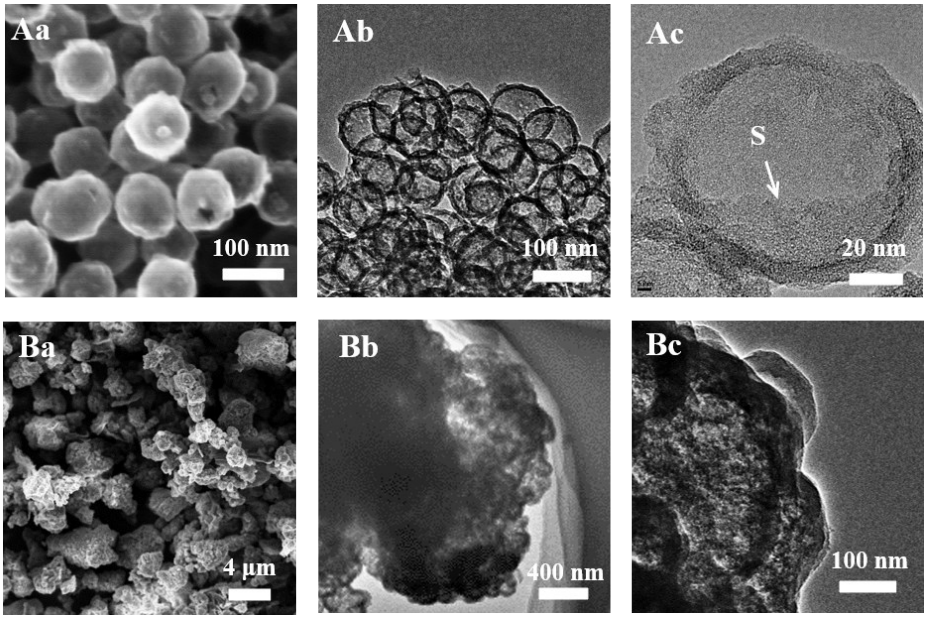

Fig. S14. (a) SEM and (b,c) TEM images of S@CG (A) and MnO_2-S@CG (B).

Note: As contrast, the S@CG was prepared through empolying hollow-CG as S host material to be with sulfur infiltration. The corresponding morphology characterization is shown in Fig. S14. As can be seen from the SEM, the composite is a monodisperse nanosphere, and the overall morphology maintains excellent dispersion. The diameter of a single microsphere is ~80 nm. The TEM images of the S@CG demonstrate the sulfur successfully permeate into the hollow sphere with the remaining space, it favors the S volume expansion in the application of lithium-sulfur batteries, and the remaining internal space can further enhance the mass loading of the S. Thus, the valid S solution infiltration strategy is convenient, which can not only effectively adjust the mass loading of S but also does not leave S block outside.

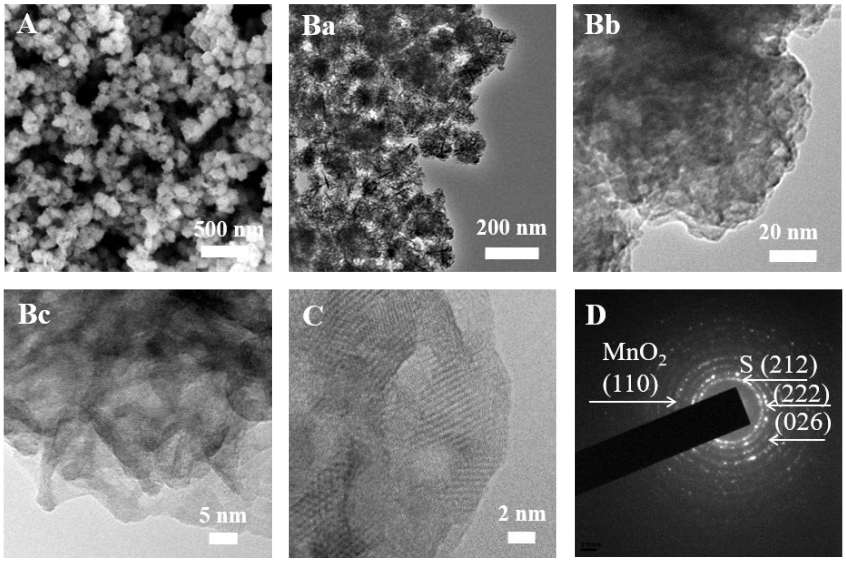

Fig. S15. (A) SEM, (B) TEM, (C) HRTEM images and (D) corresponding SAED pattern of MnO_2-S.

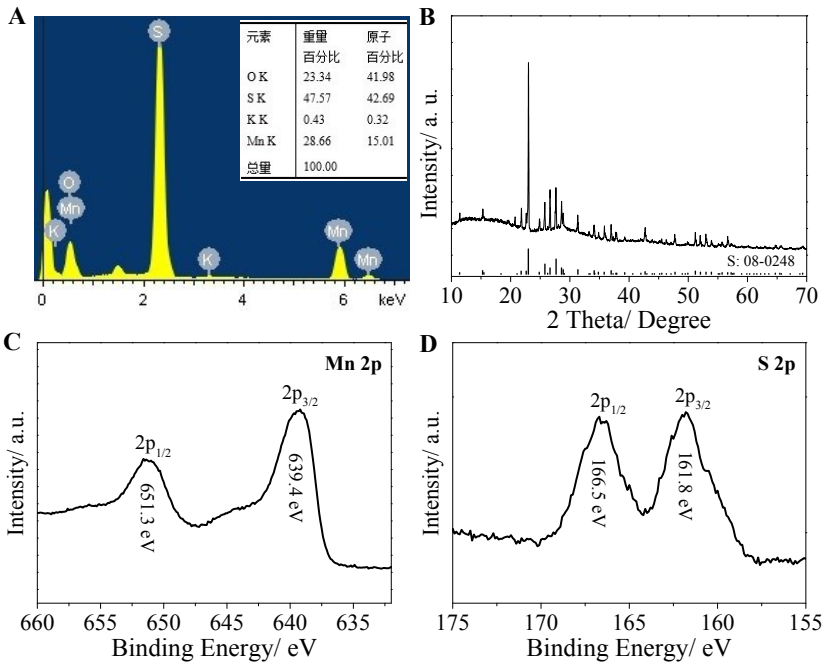

Fig. S16. (A) EDS, (B) XRD and (C, D) high-resolution spectra of Mn 2p, S2p of MnO_2-S.

Note: MnO_2-S has been prepared through a new valid S solution infiltration strategy infiltrate the S onto ultrathin-MnO_2 carrier. The corresponding morphology was shown in Fig. S15. The SEM and low magnification TEM images demonstrate that MnO_2-S remains spherical with good dispersion and no residual sulfur block, which again testify the advantages of valid S

solution infiltration strategy. Compared with the MnO_2 (Fig. S8B), the MnO_2-S clearly shows that S successfully adsorbed on the ultathin-MnO_2. In the selected area electron diffraction (SAED) pattern, the Debye-Scherrer rings corresponding to the diffractions of the (110) planes of MnO_2 and (212), (222), (026) planes of S, which predicates the existence of MnO_2 and S. According to EDS datas (Fig. S16A), the mass of S in the complex accounted for 47%. The XRD diffraction peak (Fig. S16B) is also consistent with the standard card JCPDS 08-0248 of S. Fig. S16C and S16D also show the XPS spectra of Mn 2P and S 2P, thus proving the successful load of S on ultrathin-MnO_2.

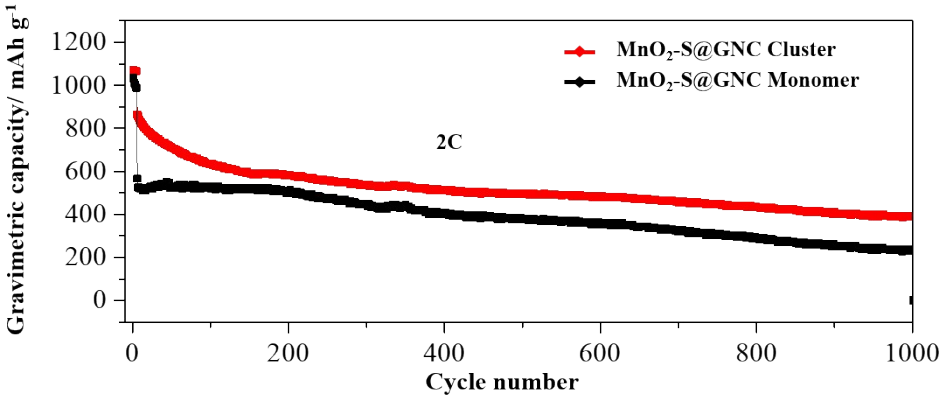

Fig. S17. Gravimetric Cycling performance of the clustered MnO_2-S@NCG. (E/S ratio: 25 µL mg^{-1}, S loading: ~2.3 mg cm^{-2}).

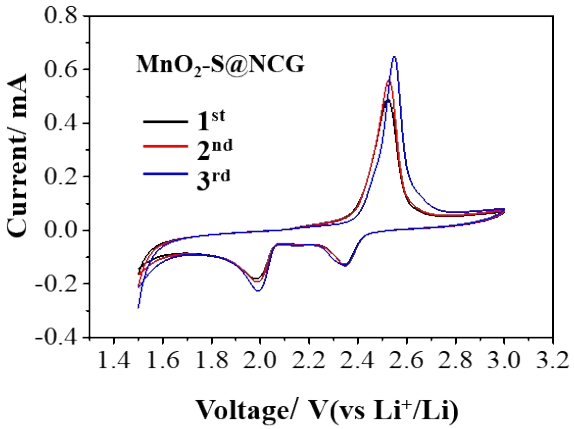

Fig. S18. Cyclic voltammograms profiles of the clustered MnO_2-S@NCG composite at scan rate of 1 mV s^{-1}.

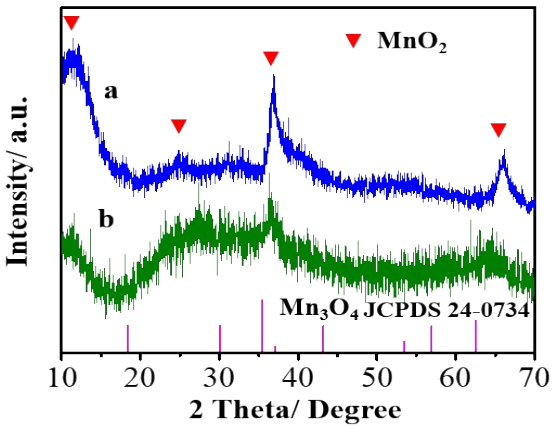

Fig. S19. XRD pattern of pristine ultrathin-MnO_2 (a) and treated with Li_2S_4 (b).

Note : To further obtain more information about the interaction mechanism between ultrathin-MnO_2 and LiPSs. The contrastive XRD pattern of pristine ultrathin-MnO_2 and treated with Li_2S_4 after 15 min in DME/DOL solution (100 mL,1:1, vol%) has been studied in Fig.S19. All the characteristic peaks of ultathin-MnO_2 were missing, while a new broad reflection peak appeared at and the peak at 2θ=36.4° is assigned to (211) plane of Mn_3O_4 hausmannite phase (JCPDS 24-0734), indicating the partially transform of ultathin-MnO_2 into new Mn_3O_4 phase. The reseason could be explained as follows: the redox reaction between ultathin-MnO_2 and LiPS lead to the Mn^{4+} reducted to Mn^{3+} and Mn^{2+}.

References

1 H. Chen, J. He, C. Zhang, H. He, *J. Phys. Chem. C* 2007, **111,** 18033-18038.

2 N. Liu, Z. Lu, J. Zhao, M. T. McDowell, H.-W. Lee, W. Zhao, Y. Cui, *Nat. Nanotechnol.* 2014, **9,** 187.

3 L. Ni, G. Zhao, G. Yang, G. Niu, M. Chen, G. Diao, *ACS Appl. Mater. Interfaces* 2017, **9,** 34793-34803.